Southern Africa Summer Drought and Heat Waves: Observations and Coupled Model Behavior

BRADFIELD LYON

International Research Institute for Climate and Society, The Earth Institute, Columbia University, New York, New York

(Manuscript received 20 February 2009, in final form 5 June 2009)

ABSTRACT

Observations of daily maximum temperature (Tx) and monthly precipitation and their counterpart fields from three coupled models from the Coupled Model Intercomparison Project Phase 3 (CMIP3) archive have been used for exploratory research into the behavior of heat waves, drought, and their joint occurrence across the southern Africa subcontinent. The focus is on seasonal drought and heat waves during austral summer [December–February (DJF)] for land areas south of 15°S. Observational results (Tx available only for South Africa) are compared with those based on CMIP3 twentieth-century climate runs for a common analysis period of 1961–2000 while climate projections for the twenty-first century are also considered using the Special Report on Emissions Scenarios (SRES) A1B forcing scenario. Heat waves were defined when daily Tx values exceeded the 90th percentile for at least 3 consecutive days, while drought was identified via a standardized index of seasonal precipitation. When assessed over the entire study domain the unconditional probability of a heat wave, and its conditional probability given drought conditions, were similar in the models and (for a smaller domain) observations. The models exhibited less ability in reproducing the observed conditional probability of a heat wave given El Niño conditions. This appears to be related to a comparatively weak seasonal precipitation teleconnection pattern into southern Africa in the models during El Niño when drought conditions often develop. The heat wave–drought relationship did not substantially change in climate projections when computing anomalies from future climate means. However, relative to a 1981–2000 base period, the probability of a heat wave increases by over 3.5 times relative to the current climate. Projections across the three models suggest a future drying trend during DJF although this was found to be a model-dependent result, consistent with other studies. However, a decreasing trend in the evaporative fraction was identified across models, indicating that evaluation of future drought conditions needs to take into account both the supply (precipitation) and demand (evaporation) side of the surface water balance.

1. Introduction

Drought is a natural manifestation of climate variability that ranks near the top of all hydrometeorological hazards in terms of the number of people it affects around the globe (Wilhite 2000). Drought occurs in virtually all climates (with the exception of semipermanent arid regions where it does not have meaning) and can lead to substantial socioeconomic and environmental impacts. During summer months drought impacts can be exacerbated by the simultaneous occurrence of heat waves that often, though certainly not always, accompany them. For example, during the 1991/92 summer drought in southern Africa it is estimated that as much as 3 million tons of grain production were lost in this predominately rain-fed agricultural region (Dilley and Heyman 1995). The extreme high temperatures that accompanied the drought not only contributed to the crop losses but also to widespread livestock mortality (Sivakumar 2006) and stresses on regional water supplies. The joint occurrence of these two climate extremes is of consequence in any region of the globe although research has largely focused on the two phenomena in isolation.

In this paper, the occurrence of seasonal drought and heat waves is examined for the subcontinent of southern Africa (land areas south of 15°S). Observational characteristics of their behavior are first considered for

Corresponding author address: Dr. Bradfield Lyon, International Research Institute for Climate and Society, Columbia University, 61 Route 9W, P.O. Box 1000, Palisades, NY 10964-8000.
E-mail: blyon@iri.columbia.edu

DOI: 10.1175/2009JCLI3101.1

the period 1961–2000 and then compared with related behavior in coupled models from the World Climate Research Programme's (WCRP) Coupled Model Intercomparison Project Phase 3 (CMIP3) multimodel dataset. The Twentieth-Century Climate in Coupled Model (20C3M) runs, which include forcing from observed aerosols and greenhouse gas concentrations are used for this purpose. The possible future behavior of drought and heat waves, considered separately and jointly, are then evaluated using the same CMIP3 models forced with the Special Report on Emissions Scenarios (SRES) A1B greenhouse gas scenario where CO_2 concentrations reach a maximum of 720 ppm during the twenty-first century. While a general agreement (should it be found) between observed and modeled characteristics of drought and heat waves will obviously not guarantee the fidelity of model projections of future climate, this study provides a reference level of model performance. In addition, the joint occurrence of these two climate extremes is of interest in its own right, independent of climate change.

The tendency for summer rainfall and surface air temperature over land to be negatively correlated is well known (Madden and Williams 1978; Huang and van den Dool 1993; Trenberth and Shea 2005; Déry and Wood 2005, and many others). The physical linkage is via the surface energy budget with below-average precipitation typically associated with reduced soil moisture and increased insolation with both favoring an increase in the surface sensible heat flux and therefore higher surface air temperature. The full picture is somewhat more nuanced, as it is the net surface radiation, which serves as a control on surface evaporation and soil moisture is more closely tied to the evaporative fraction than to evaporation itself and this relationship is sensitive to the local soil moisture "regime" (e.g., Koster et al. 2009). Nonetheless, land surface–atmosphere interaction likely plays an important role in the joint occurrence of the two phenomena.

In southern Africa this behavior is often seen, for example, during El Niño–Southern Oscillation (ENSO) events, which tend to be associated with a near-synchronous occurrence of deficient rainfall and elevated surface air temperatures on the seasonal time scale (Ropelewski and Halpert 1987; Halpert and Ropelewski 1992). However, the relationship between shorter periods (i.e., several days) of extreme high temperatures (heat waves) and the occurrence of drought is less clear as daily maximum temperatures are also affected by variations in cloud cover, proximity to large water bodies, prevailing wind direction, thermal advection, etc.

The joint occurrence of summer heat waves and drought is also confounded by the prospect of climate change. For example, climate change scenarios are in general agreement that land surface temperatures will increase in the twenty-first century, generally increasing the probability of extreme daily temperatures (though not necessarily in a spatially uniform manner, e.g., Meehl and Tibaldi 2004). Yet these same models can diverge considerably in their projected changes in precipitation, which in the case of southern Africa during summer has some showing a drier, and others wetter, climate relative to the twentieth century (Solomon et al. 2007, see their Fig. 11.2, p. 869). Therefore, in the coming decades there could potentially be more heat waves even in regions with upward trends in rainfall (in the absence of drought), or decreased precipitation may lead to more frequent droughts, favoring the joint occurrence of heat waves via changes in surface heat fluxes.

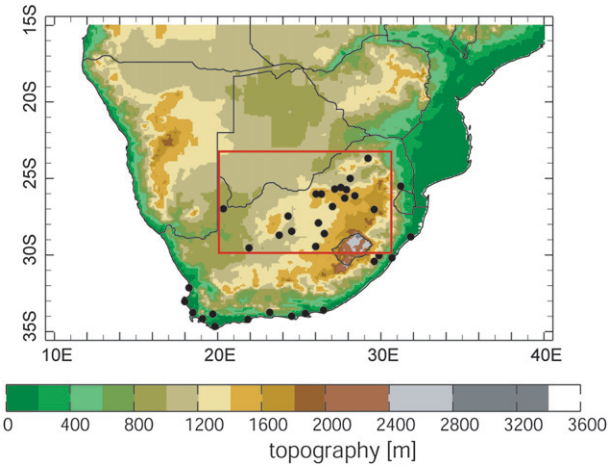

FIG. 1. Location of stations with daily Tx observations used in the study (filled circles). Topographic relief is shaded and the red rectangle indicates the domain for stations used to compare with 20C3M model results shown in Figs. 3 and 7.

The paper is outlined as follows. The basic datasets used and methodological approach taken are described in section 2. The observational results and their comparison with 20C3M runs are then discussed in section 3, followed by analyses from the climate change projections in section 4. Section 5 contains an overall summary and the main conclusions from the study.

2. Data and methodological approach

a. Observational data

Daily maximum temperatures (Tx) from 92 stations across South Africa were obtained from the South African Weather Service. To be used in the analysis here these stations had to have at least 95% complete observational records for the months of December–February (DJF) over the period 1961–2000. A total of 35 stations met this restriction and their locations are shown in Fig. 1. The daily Tx station data were also used to compute

TABLE 1. Coupled models used in the study.

Model name	Modeling group	Country	Approximate resolution lat × lon (°)
CSIRO-Mk3.5	CSIRO Atmospheric Research	Australia	1.8° × 1.875°
ECHAM5/MPI-OM	Max Planck Institute for Meteorology	Germany	1.8° × 1.875°
GFDL-CM2.0	U.S. Dept. of Commerce/NOAA/Geophysical Fluid Dynamics Laboratory	United States	2.0° × 2.5°
Additional			
CNRM-CM3	Météo-France/Centre National de Recherches Météorologiques	France	2.8° × 2.8°

monthly and seasonal values of Tx. Monthly, gridded analyses of precipitation based on station observations were obtained from the World Climate Research Program (WCRP) Global Precipitation Climatology Center (GPCC; Rudolf and Rubel 2005). These data are gridded to a 0.5° spatial resolution. Gridded, monthly average surface air temperature data at 5° spatial resolution were from the University of East Anglia (Jones and Moberg 2003), while monthly, global fields (2.0° resolution) of sea surface temperature (SST) were from the extended reconstructed dataset (Smith and Reynolds 2004) version 2. Finally, various atmospheric fields from the National Centers for Environmental Prediction–National Center for Atmospheric Research (NCEP–NCAR) reanalyses were used (Kistler et al. 2001).

b. *Coupled model data*

A summary of the coupled climate models utilized in the study is provided in Table 1. Model output fields were obtained from the archives at the Program for Climate Model Diagnosis and Intercomparison (PCMDI) Web site (available online at http://www-pcmdi.llnl.gov/). Both 20C3M runs and climate change projections based on runs forced with the A1B greenhouse gas scenario were utilized. The 20C3M simulations incorporate known natural and anthropogenic forcings including aerosols and volcanoes as well as major greenhouse gas concentrations. Several model fields were employed including daily maximum temperature data for identifying heat waves and monthly precipitation for analysis of drought. It is beyond the scope of this paper to examine the behavior of heat waves (and drought) across all the CMIP3 models. The selection of the three primary models used here was instead based on their general ability to generate realistic ENSO characteristics (e.g., AchutaRao and Sperber 2006) while also having daily Tx (and other) data available for both the 20C3M and A1B runs. ENSO teleconnections in the models, including drought in southern Africa was further examined by first applying empirical orthogonal function (EOF) analysis to tropical Pacific (25°S–25°N, 180°–80°W) SST averaged over the DJF season (not shown). The upper and lower quartile values of the associated principal component (PC) time series were then used as thresholds to identify ENSO events, a definition used throughout this paper. An EOF analysis of the 3-month standardized precipitation index (SPI; McKee et al. 1993) was then performed based on model rainfall for all Southern Hemisphere land areas (10°N–55°S). The leading EOFs of both the SST and SPI fields related to ENSO had temporal correlations between the respective PC time series ranging from roughly 0.8 to 0.9 across the models. The loading patterns of first EOF of the DJF SPI index (Fig. 2) reveals that the models generally capture the ENSO teleconnection pattern over southern Africa seen in observations (Fig. 2a) although there are variations in the spatial pattern across models.

c. *Defining heat waves and drought*

A heat wave was defined as a period of at least 3 consecutive days when the daily Tx exceeds the 90th percentile during the DJF season. A minimum of 5 consecutive days and/or the 95th percentile criteria were also examined but did not substantially alter the results (other than to identify fewer cases); the results are not reported here. The Tx percentiles were obtained by ranking the daily data over all DJF seasons for the periods 1961–2000, 1981–2000, 2046–65, and 2081–2100 depending on the analysis. Percentiles were used rather than absolute values of Tx because of variations in temperature associated with local station (or model grid point) elevations, etc. The heat wave definition used here is deemed relevant in terms of impacts as previous studies have found that even a few days of extreme temperatures can have major consequences for humans, livestock, and terrestrial biota generally (Kalkstein and Davis 1989; Changnon et al. 1996; Parmesan et al. 2000; Basu and Samet 2002; Argaud et al. 2007). Previous work has also shown that the joint occurrence of drought and heat waves can exacerbate related impacts [e.g., in African cattle (Kay 1997), and agriculture (Dilley and Heyman 1995)]. The definition of a heat wave used in this study is similar to that used in other studies (e.g., Meehl and Tibaldi 2004).

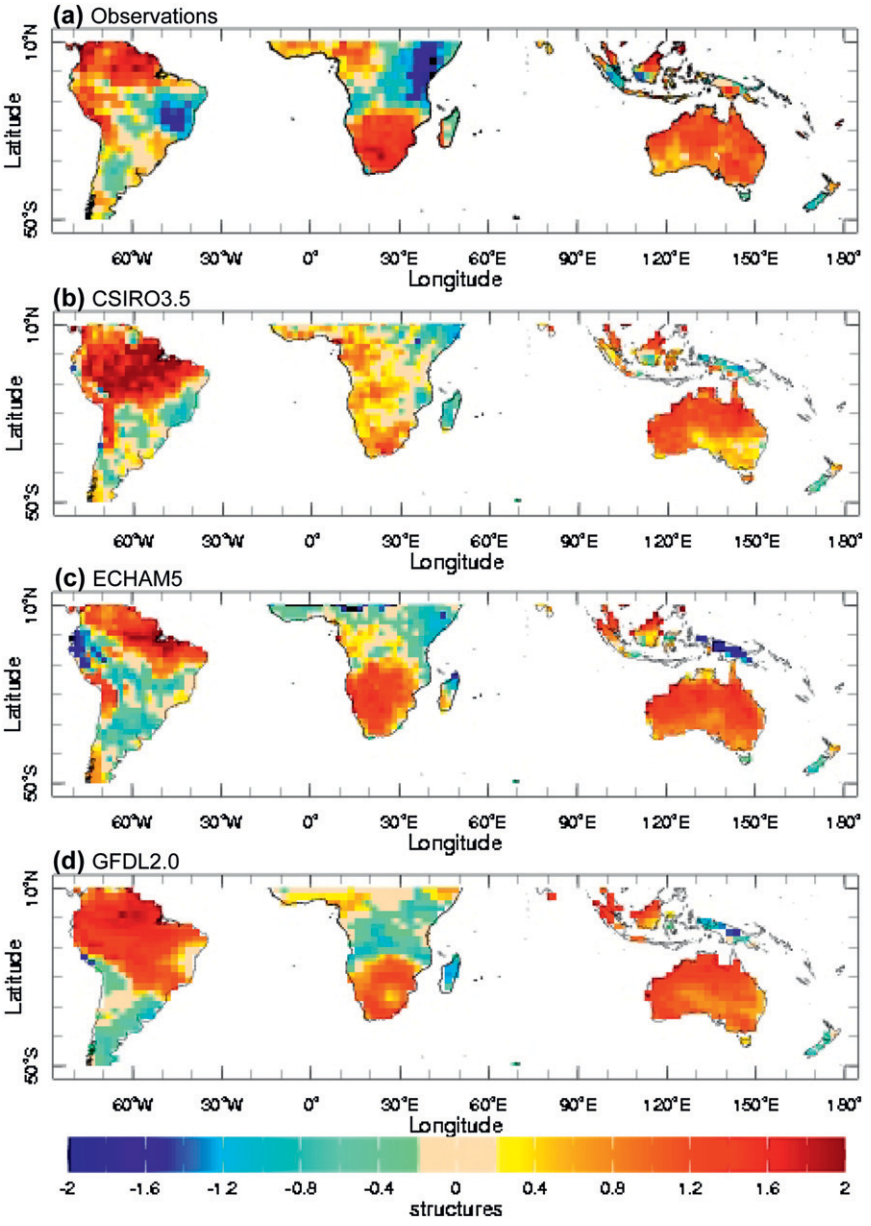

FIG. 2. Loading patterns (dimensionless, sign arbitrary) of the first EOF of the SPI index evaluated for the DJF seasons (1961–2000) for observations based on (a) monthly GPCC precipitation data, (b) CSIRO3.5, (c) ECHAM5, and (d) GFDL2.0.

Drought was primarily defined using a weighted anomaly standardized precipitation index (WASP; Lyon 2004; Lyon and Barnston 2005) although the SPI (McKee et al. 1993) was also utilized. The WASP and SPI are highly correlated (based on the GPCC data, the area-average temporal correlation for southern Africa land area grid points south of 15°S for DJF is $r = 0.95$). A benefit of the WASP index is its flexibility for use in the analysis of changes in drought characteristics in climate change scenarios discussed in section 4. Essentially, the WASP index is based on the weighted sum of standardized, monthly precipitation departures from the average:

$$S_n = \sum_{i=1}^{n} \frac{\sqrt{P_i} - \overline{\sqrt{P_i}}}{\sigma_{\sqrt{P_i}}} \frac{\overline{P}_i}{\overline{P}_A}, \tag{1}$$

where P_i is precipitation for the ith month in the sum, overbars represent climatological mean values, the subscript A denotes annual value, and σ_i is the standard deviation of precipitation for the ith month in the sum.

The square root is taken to reduce the positive skewness that is often associated with precipitation observations and the last term is a weighting factor to reduce the value of the standardized anomalies during seasonally dry months. Since seasonal droughts are emphasized here, a 3-month sum is considered (i.e., $n = 3$). The sum in Eq. (1) is then standardized based on its historical variability for the given 3-month season considered (e.g., DJF). For observational data the climatological base period used was 1961–2000 and the frequency distribution of the index is approximately normal.

For model data the evaporative fraction, EF, was computed as

$$\mathrm{EF} = \frac{1}{1+B}, \quad \text{where } B = \frac{\mathrm{SH}}{\mathrm{LH}}. \tag{2}$$

In Eq. (2), SH and LH are the surface sensible and latent heat fluxes, respectively, with B representing the Bowen ratio.

d. Unconditional and conditional probabilities

The unconditional probability of outcome X was computed as the relative frequency of occurrence of X over the period considered (e.g., 1960–2000). Conditional probabilities were computed in two ways. One approach was again to compute the relative frequency of occurrence X given condition Y. A second approach was to use the parameters of a bivariate normal distribution, namely the means (μ_X and μ_Y) and standard deviations (σ_X and σ_Y) of the two variables (X and Y) and their correlation (ρ). The conditional distribution of X given a particular value of Y then has parameters given by (Wilks 1995)

$$\mu_{X|Y} = \mu_X + \rho\sigma_X \frac{(y - \mu_Y)}{\sigma_Y}, \tag{3}$$

$$\sigma_{X|Y} = \sigma_X \sqrt{1 - \rho^2}. \tag{4}$$

The frequency distributions of both Tx and the WASP index are approximately normal making them amenable to this approach.

3. Observational period (1961–2000) and 20C3M results

a. Conditional distributions of Tx anomalies based on drought state

As a starting point, conditional probability distributions of standardized Tx anomalies were computed based on the simultaneous occurrence of drought for both station data and 20C3M coupled model output for the 1961–2000 period. Different time scales were considered including monthly and seasonal averages of Tx. The Tx data were standardized by first computing the (i.e., monthly–seasonal) departures from their associated long-term mean (i.e., 1961–2000) for a station or model grid point and then dividing by the standard deviation of Tx computed over the same base period for the time scale of interest (i.e., monthly–seasonal). For monthly temperatures, drought conditions were identified when the 1-month WASP index was less than −1.0. For seasonal temperature data the value of the 3-month WASP index in February was used. In observations the drought index was computed from the GPCC gridded precipitation data with the nearest grid point to a given station used in the analysis. The model data included all land area grid points south of 15°S, with the Geophysical Fluid Dynamics Laboratory Climate Model version 2.0 (GFDL CM2.0) data for the smaller domain (approximately the ''boxed'' region in Fig. 1) also used for comparison with observations. The stations within the boxed region of Fig. 1 were selected for being generally away from coastal locations where local factors relating to topography and oceans affect heat wave occurrence, as discussed further in section 3b.

The results (Fig. 3) indicate the strongest relationship between Tx anomalies and drought, in both observations and the models, occurs on the seasonal time scale with a tendency for more frequent occurrences of above-average Tx values during drought. When averaged over a month or a season the effects of daily weather conditions on Tx tend to cancel allowing the weaker, but consistent, influence of drought conditions to show up more clearly. Heat waves, as defined in the current study, occur relatively infrequently (the 90th percentile in daily Tx is expected to be reached, on average, less than 10 days over an entire season). Nevertheless, over a sequence of just a few days (here three or more) the existence of drought (and anomalous land surface conditions) can favor higher daily Tx values leading to heat waves.

b. Unconditional and conditional probabilities for heat waves based on drought and ENSO state in observations

Daily Tx data from the 35 stations were used to assess the unconditional probability of a heat wave occurring during a given month of the DJF season based on Tx percentiles computed over the 1961–2000 base period. The distribution of probabilities across all stations was computed for the subperiods 1961–80 and 1981–2000 (Fig. 4a). The mode of both distributions is around 25%–30% although there is a clear shift in the more recent period toward higher probabilities for heat waves. The increase in heat wave frequency in recent

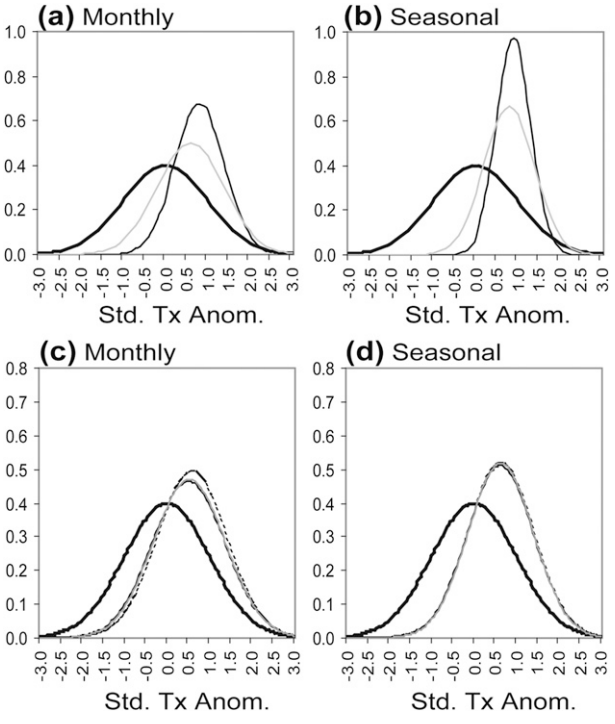

FIG. 3. Frequency distributions of standardized Tx anomalies for different averaging periods conditioned on the existence of drought (3-month WASP index < -1.0) for the period 1961–2000. The thick black line on the plots represents the unconditional distributions. Station locations are within the ''boxed'' region in Fig. 1; model results are for all land area grid points in southern Africa south of 15°S. Results for observations and 20C3M runs, respectively, are shown for (a),(c) monthly values and (b),(d) seasonal values. Results from the GFDL2.0 model for a spatial domain similar to observations are also shown in (a),(b) as a thin gray line.

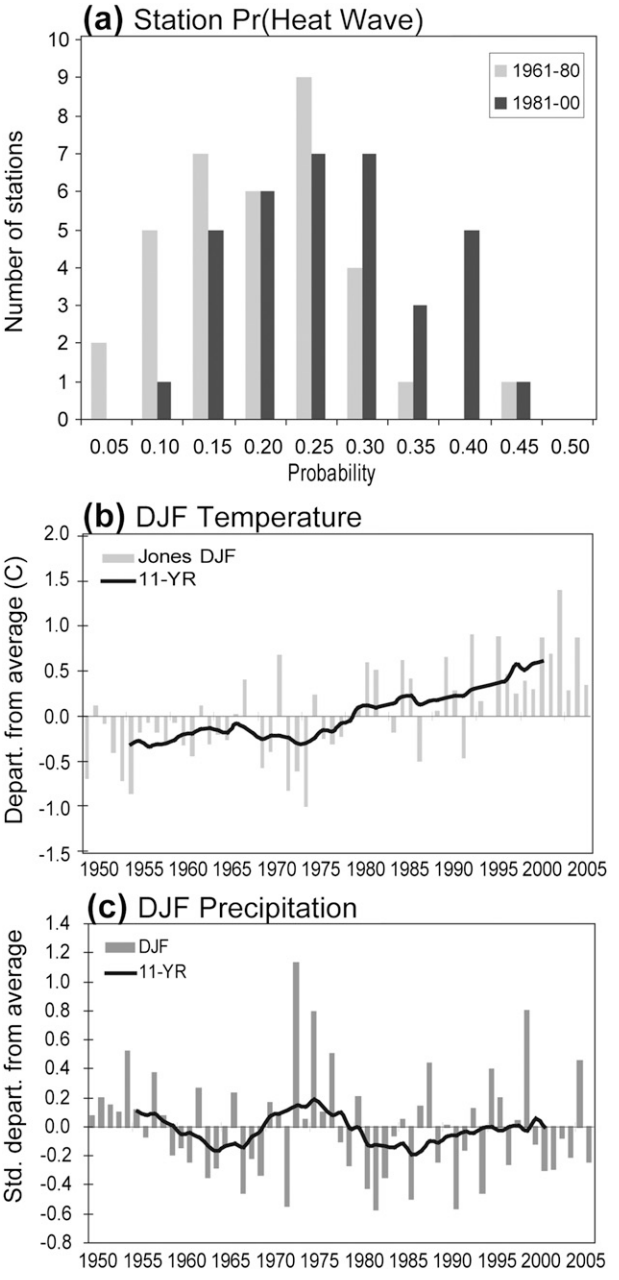

FIG. 4. (a) Number of stations in different unconditional probability categories of having at least one heat wave during the DJF season for the periods 1961–80 (light gray bars) and 1981–2000 (dark gray). (b) Area-averaged DJF temperature departures from a 1961–2000 base period mean (°C) for southern Africa (land area grids points south of 15°S) are indicated by bars with an 11-yr running average value indicated by the black line. (c) Same as (b), but for standardized departures of DJF precipitation (dimensionless) for the same domain.

years is most likely associated with an observed upward trend in surface air temperature during the DJF season in recent decades (Fig. 4b) and is a finding consistent with other studies (Kruger and Shongwe 2004; Alexander et al. 2006).

The possible influence of urbanization (i.e., heat island effects) on the upward trend in heat waves is a consideration here. For the period 1960–90, Hughes and Balling (1996) suggested that upward (downward) trends in the mean daily temperature (diurnal temperature range) were generally greater for the 5 urban versus 19 nonurban stations they examined for South Africa. However, their examination of Tx trends did not show similar differences with location. Using daily station data for South Africa extending through 2003, Kruger and Shongwe (2004) suggest that, with the exception of Pretoria, urbanization effects on Tx were not substantial with most of the 26 stations they considered being sufficiently far away from urban centers. In the current analysis a shift toward higher heat wave occurrence in recent years occurs over all 35 stations (many in nonurban areas), suggesting that urbanization is not the driver of the shift. Similar results were found using a subset of

stations (total of 17) that were more evenly spaced across the domain shown in Fig. 1.

Since the relationship between temperature and precipitation is the focus of the study, the GPCC data for all land areas south of 15°S were used to examine interannual variability in DJF rainfall. Given the large climatological variations in rainfall across the region, for this analysis DJF rainfall was first expressed as a standardized departure from the 1961–2000 average at each grid point before the spatial averaging was computed. The results (Fig. 4c) mainly indicate large interannual and decadal variability in precipitation without any clear secular trend. Some other studies have suggested there has been a downward trend in precipitation over various parts of southern Africa, particularly since the late 1970s (Mason and Tyson 2000 and references therein), along with an increase in interannual rainfall variability. Figure 4c does suggest greater interannual variability in DJF precipitation since the 1970s.

The spatial distribution of the unconditional probability of a heat wave occurring during a given month during DJF is shown in Fig. 5a. The conditional probability based on drought conditions, identified when the December, January, or February value of the 3-month WASP index was <-1.0, is shown in Fig. 5b with the conditional probability for El Niño years displayed in Fig. 5c. Higher probabilities of heat waves conditioned on drought are largely seen in interior sections of South Africa, away from coastal locations. These inland areas also show enhanced heat wave probabilities during El Niño events, which are often accompanied by drought as well as above-average tropospheric temperatures during austral summer (e.g., Lyon and Mason 2007). Kenyon and Hegerl (2008) have recently shown how large-scale modes of climate variability such as ENSO can influence the occurrence of temperature extremes on a global basis. Their results included an increase in the number of warm days in southern Africa during El Niño events in austral summer. The spatial variations in heat wave probabilities (during drought and/or ENSO events) across stations are interesting in their own right and were examined in a bit more detail.

First, EOF analysis was first applied to the 3-month SPI index for the DJF season across the southern Africa domain. The loading pattern (Fig. 6a) of the leading EOF (explaining 28% of total variance) indicates weights of the same sign across almost all the domain (as in Fig. 2a). The temporal correlation between the associated first principal component time series and time series of SST anomalies averaged over the Niño-3.4 region (5°S–5°N, 120°–170°W) is $r = 0.64$, statistically significant at greater than 95% confidence. Anomalous 850-hPa horizontal wind components for the DJF season in the reanalysis were regressed onto this first PC time series with results plotted in Fig. 6b. The anomalous wind vectors have a pattern similar to that of ENSO composites for the same season (not shown). Anomalous westerly low-level flow across the comparatively cool

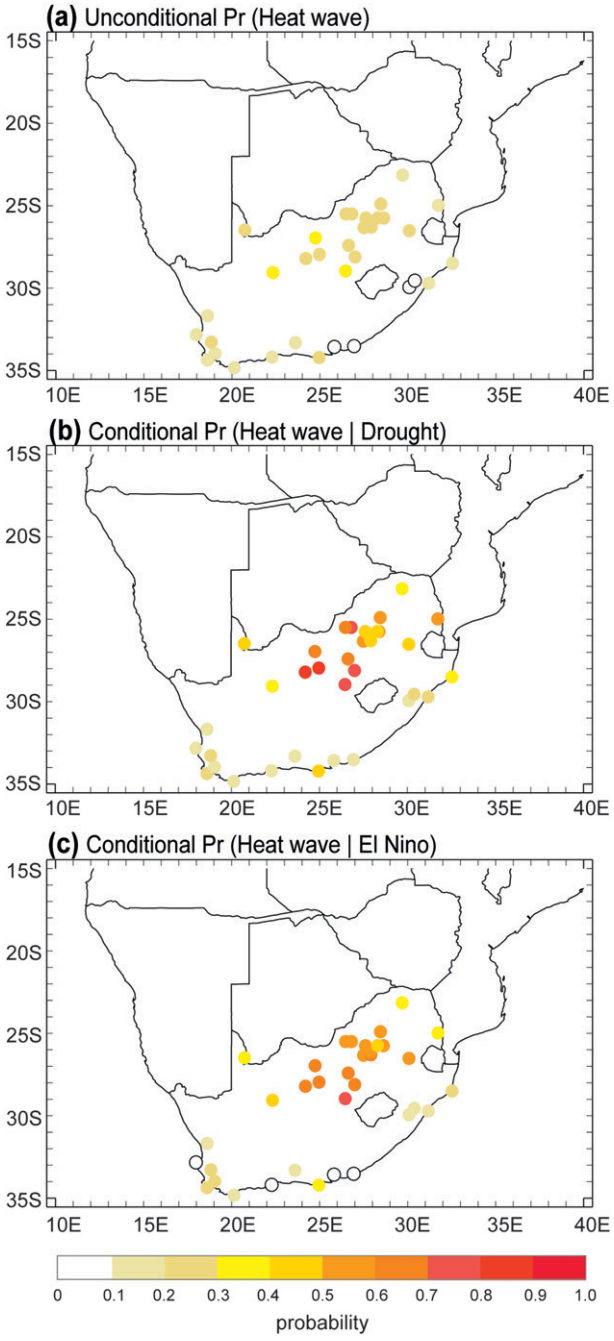

FIG. 5. (a) Unconditional probability of at least one heat wave during the DJF season (1961–2000) for all stations. (b) The conditional probability of a heat wave given drought conditions. (c) The conditional probability of a heat wave given an El Niño event.

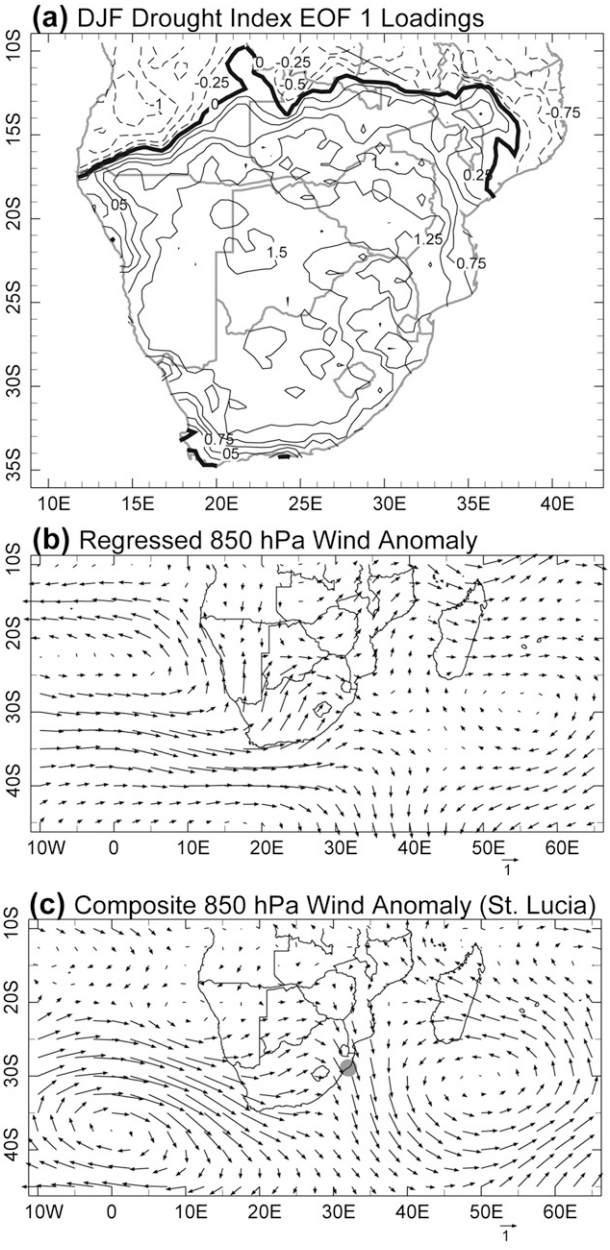

FIG. 6. (a) Loadings (dimensionless, sign arbitrary) of the leading EOF of the 3-month SPI for DJF (1961–2000). (b) Anomalous 850-hPa reanalysis winds for the DJF season regressed onto the PC time series associated with the EOF pattern in (a). (c) Composite 850-hPa daily wind anomalies during 19 heat wave events at Cape St. Lucia (filled circle). Reference wind vectors (m s^{-1}) are shown at lower right of (b) and (c).

southeast South Atlantic Ocean into the western and southern parts of South Africa is consistent with relatively small probabilities of heat waves during drought (including El Niño–related drought). In marked contrast, Fig. 6c shows a composite of 850-hPa reanalysis daily wind anomalies during 19 heat wave events that occurred at St. Lucia (location given by gray dot in figure) between 1961 and 2000. Northwesterly, downslope flow is implied at that location. Similarly unique composites for other coastal locations (not shown) indicated the importance of steep local topography and adiabatic descent (''Berg,'' or foehn, winds) for the development of heat waves in such coastal locations. It is for this reason that coastal locations were not included in the station analysis of drought–Tx relationships shown in Fig. 3. A more detailed analysis of local factors and physical processes influencing heat wave generation in coastal locations of southern Africa would be insightful but goes beyond the scope of the current study.

c. 20C3M coupled model results (1961–2000)

Unconditional and conditional probabilities of heat wave occurrence in the 20C3M runs were computed in a similar fashion to that using observational Tx data. All model grid points over land areas south of 15°S were used in the analysis. Drought occurrence in a given month was again defined when the 3-month WASP index was <-1. El Niño events in the models were defined based on DJF SST anomalies averaged across the Niño-3.4 region in the models being in the upper quartile of the historical distribution. The model results are summarized in the histograms shown in Fig. 7, which also provides summaries based on observational data for comparison.

The distributions of the unconditional probability of a heat wave across the southern Africa domain for all three models are quite similar to observations (the latter for the boxed domain in Fig. 1). The mode in the frequency of occurrence in both models and observations is a 25% probability. The conditional probability of a heat wave given drought conditions (Figs. 7c,d) increases substantially from the unconditional values across the models. While there are intermodel differences in these probabilities, overall the distributions are again quite similar to observations. Therefore, generally speaking, the models appear to be capable of generating the observed characteristics of unconditional and conditional probabilities of heat waves across southern Africa. There are the caveats that 1) the spatial domains for the observations and model data overlap, but are not the same and 2) the spatial patterns of heat waves and drought in the models and observations are not considered and may in fact display differences. This second point is not considered here as the general behavior of the models across the entire domain is the emphasis of the current study.

The conditional probability of a heat wave given El Niño conditions in the models (Fig. 7f) shows a shift

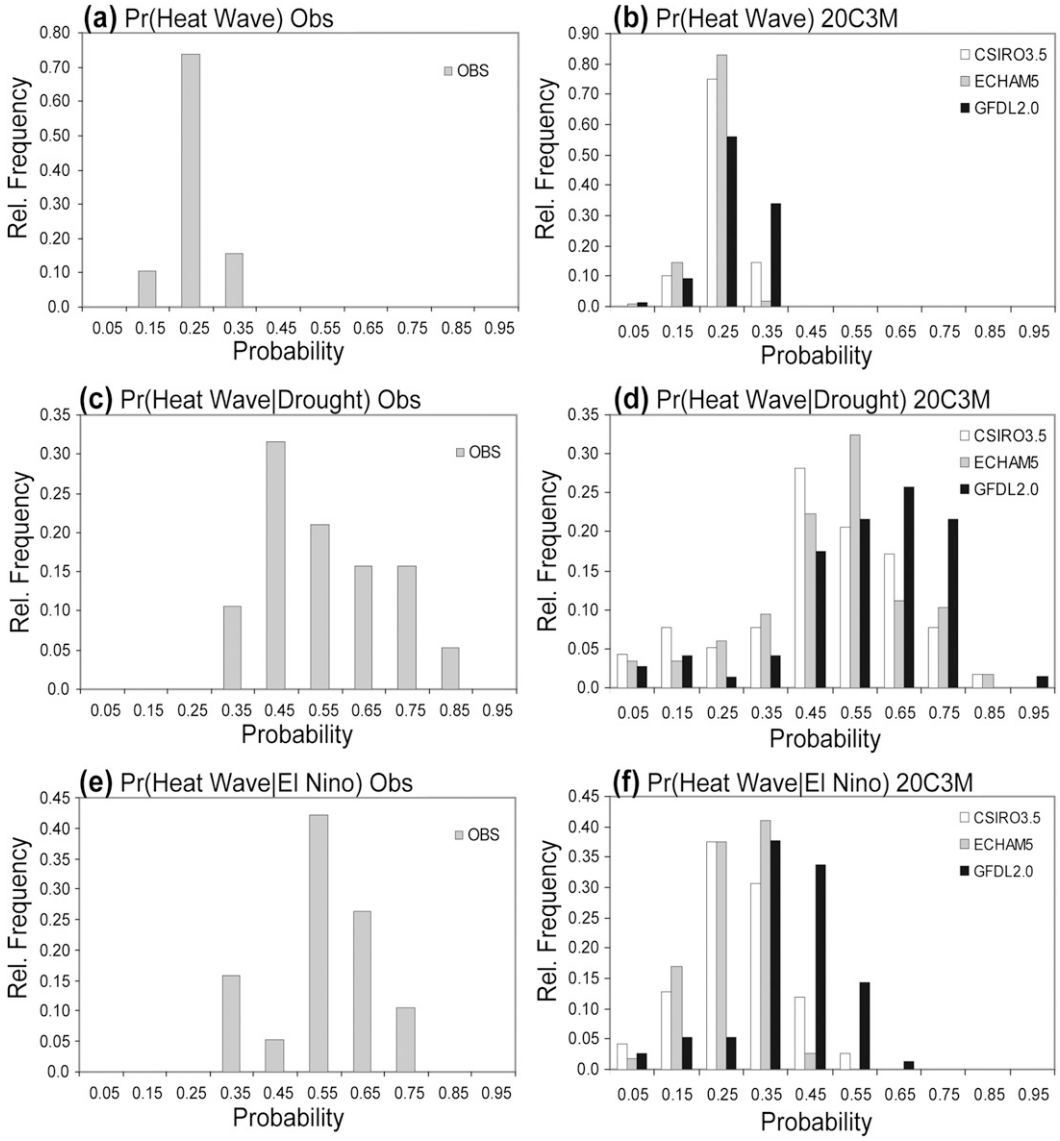

FIG. 7. (a) Relative frequency distributions of the unconditional probability of a heat wave for stations in the ''boxed'' region of Fig. 1. (b) As in (a), but for 20C3M runs and all land area grid points south of 15°S. (c),(d) Similar conditional probabilities given drought, while conditional probabilities based on El Niño conditions are given for (e) observations and (f) models.

toward higher probabilities from the unconditional values (Fig. 7b) but not as strong a shift as in observations. Given the similarities in the conditional probabilities of a heat wave given drought conditions in the models and observations, this suggests that while the drought–heat wave relationship in the models is robust in general (i.e., without consideration of ENSO), the relationship between El Niño and the development of drought cross southern Africa in DJF may be less so. This latter point is suggested, for example, in the differences in EOF loading patterns for the DJF 3-month SPI across southern Africa (in Fig. 2) between the models and observations. The EOF loadings are generally smaller in the models than in observations, with the spatial patterns of the model loadings also showing departures from the observed. This result has implications for the ability of the models to capture some aspects of possible future changes in the heat wave–drought relationship in southern Africa for even if the models capture the future behavior of ENSO ''correctly'' they may not communicate this properly to southern Africa via teleconnections.

4. Model projections (A1B forcing)

a. Model trends in temperature, precipitation, and evaporative fraction

Before examining the relationship between heat waves and drought in climate model projections, an evaluation of possible changes in projected DJF precipitation and temperature for the southern Africa subcontinent was assessed. It is noted at the outset that the following analyses are based on the raw output from the coupled models and therefore do not represent a detailed downscaling methodology. In addition, only three models are considered and therefore may not represent the range of possible future outcomes. Future changes in the character of precipitation (e.g., less frequent but more intense rainfall), including their spatial variability (e.g., Tadross et al. 2005), are not captured by seasonal means.

These caveats aside, averaged across all land area grid points in southern Africa south of 15°S, Fig. 8a shows the projected changes in area-average surface air temperature for the DJF season as departures from a 2000–2100 period mean. An 11-yr moving average was also applied. The trends in DJF temperature are similar across the models and indicate an increase of roughly 3°–4°C by the end of the twenty-first century. For precipitation (Fig. 8b) there is considerably more decadal-scale variability than for temperature but also some suggestion of a downward trend. Based on the average of 21 CMIP3 models, there is some indication of a slight downward trend in DJF precipitation in southern Africa but also substantial variation among models with roughly half the models generating wetter-than-average conditions (Solomon et al. 2007). Some studies provide indications that southern Africa lies generally within a much broader region of subtropical drying in climate projections under a similar forcing scenario (e.g., Held and Soden 2006). How projected changes in monthly precipitation during DJF relate to drought index changes will be considered in more detail in section 4c.

Finally, using the surface latent and sensible heat fluxes in the models, changes in the evaporative fraction (EF) were also considered (Fig. 8c) and expressed as a percent change from the 2000–2100 average. Again, an 11-yr running average was applied. An increase (decrease) in EF is associated with an increase (decrease) in the surface latent heat flux relative to the sensible heat flux. In all three models there is a projected downward trend in EF on the order of 4%–5% over the next century. Since EF relates directly to the surface energy balance, decreasing values of EF favor increases in surface air temperatures (and, presumably, heat waves).

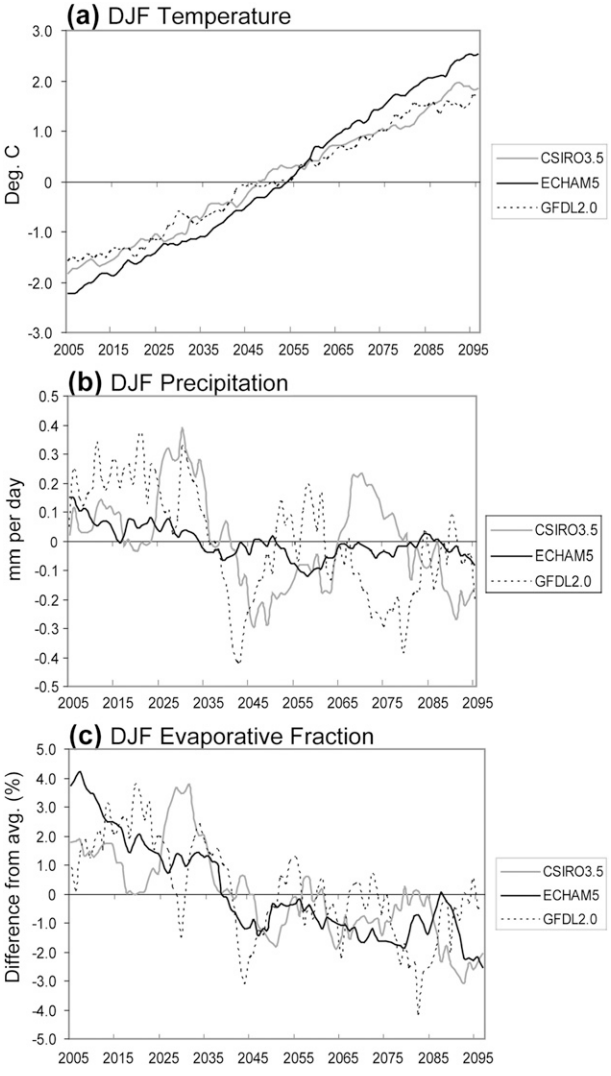

FIG. 8. A1B runs showing 11-yr running averages of departures from the 2000–2100 period mean for DJF values of (a) surface air temperature (°C), (b) precipitation (mm day^{-1}), and (c) EF (dimensionless). All plots represent area averages across all land area grid points south of 15°S. Values for the ECHAM5 model are based on the mean of four ensemble members.

b. Conditional and unconditional probability of heat waves: 2046–65 and 2081–2100

Heat waves were defined as previously but based on Tx percentiles determined by ranking daily values over DJF seasons for the separate periods of 2046–65 and 2081–2100. To examine how heat waves may change in these projections from the current climate, the 90th percentile threshold of daily Tx for the base period 1981–2000 in the 20C3M runs was also computed for all grids points across southern Africa. The 3-month WASP index was again used to identify drought during the DJF season with the climatological value of precipitation also

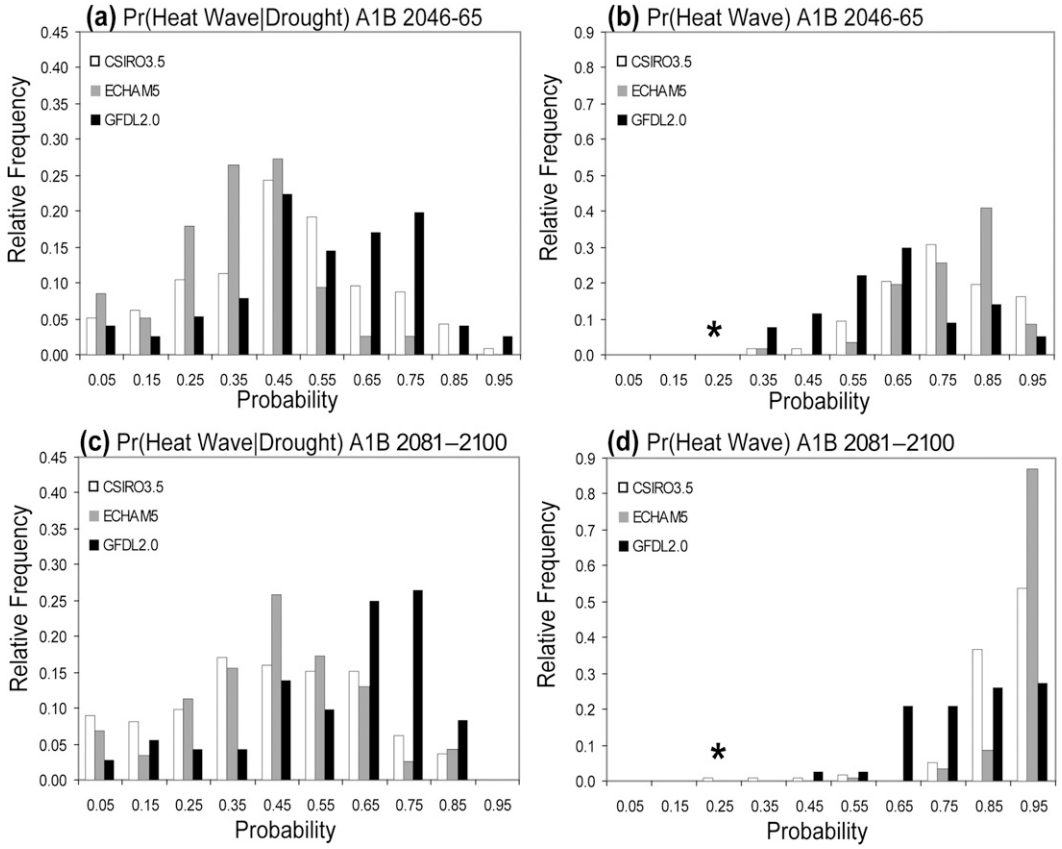

FIG. 9. As in Fig. 7, but for the conditional probability of a heat wave given drought in the A1B runs for the periods (a) 2046–65 and (c) 2081–2100. (b),(d) The unconditional probabilities of a heat wave for the same periods are shown, but computed relative to a 1981–2000 base period climatology. The asterisks indicate the modal value for the 20C3M runs shown in Fig. 7b.

computed separately for the two analysis periods. Monthly values of the WASP index <-1.0 were again used to identify drought conditions.

The frequency of occurrence (across all grids points) for the conditional probability of a heat wave given drought conditions for the 2046–65 period (Fig. 9a) is generally similar to that for the 20C3M runs (cf. Fig. 7d). Note that the two sampling periods are of different length with 40 seasons included for 20C3M runs versus 20 for the A1B runs considered here. The same general conclusion holds for the conditional probability of a heat wave given drought conditions for the 2081–2100 period (Fig. 9c). What shows a dramatic upward shift is the unconditional probability of a heat wave for these two periods when assessed using the 1981–2000 DJF base period climatology (Figs. 9b,d). In both observations and the 20C3M model runs the most frequent occurrence of the unconditional probability of a heat wave occurring in any given month was 25%. For the period 2046–65 this increases to at least 65% and for the 2081–2100 period to 95%. Thus, the unconditional probability of a heat wave increases by more than a factor of 2 by 2065 to almost 4 times by 2100 across the three model projections.

c. *Projected changes in the occurrence of drought*

Using the mean and standard deviation of monthly precipitation computed from the 1961–2000 base period in the 20C3M runs, monthly values of the 3-month WASP index were computed for the A1B model projections to evaluate any changes in the frequency distributions of the index for the DJF season. The relative frequency of occurrence of WASP index values is shown as bars in Fig. 10 with the solid line representing a normal distribution based on the 1961–2000 20C3M data. For the three main models used in the study, all show a shift toward a greater occurrence of negative drought index values (i.e., greater occurrence of drought). This was the case for both the 2046–65 and 2081–2100 periods. As mentioned earlier, there is substantial spread across the CMIP3 models regarding changes in DJF precipitation in southern Africa. An example of this is

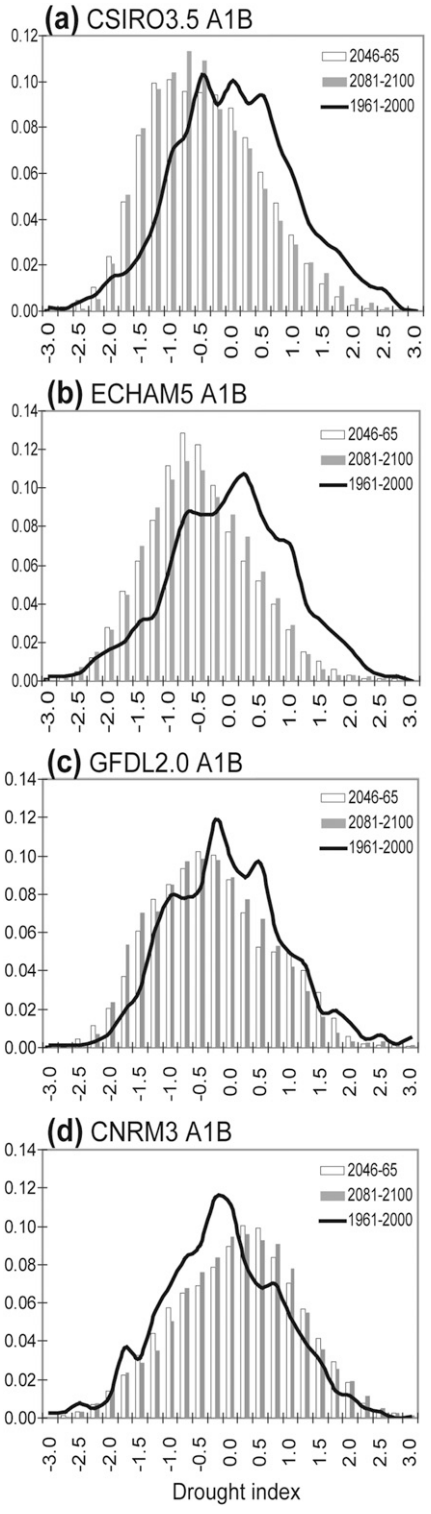

FIG. 10. Frequency distributions of the 3-month WASP index computed from A1B run monthly precipitation but using 20C3M climatological values from the 1961–2000 base period with white (gray) bars indicating the 2046–65 (2081–2100) period for (a) CSIRO3.5, (b) ECHAM5, (c) GFDL2.0, and (d) CNRM3. Thick black lines show results for the 1961–2000 base period for each model.

shown in Fig. 10d, which is based on the CNRM model and shows a slight shift toward wetter conditions relative to the 1961–2000 base period. Again, as indicated in the Fourth Assessment Report (Solomon et al. 2007), roughly half of the CMIP3 models (based on the A1B forcing scenario) indicate drying for DJF relative to 1980–99 observed climate with the other half wetter for the period 2080–99.

Although the WASP index is based solely on precipitation, the results found here are consistent with other recent studies examining changes in drought in climate change projections. For example, using soil moisture content from 15 CMIP3 models and the A1B forcing scenario Wang (2005) finds an increase in the occurrence of agricultural drought in several places around the globe including southern Africa. Similarly, using percentile values of global soil moisture from eight CMIP3 models Shefield and Wood (2008) indicate an upward trend in drought occurrence in the coming century, including southern Africa. These two studies are consistent with the finding reported here of downward trends in the value of EF in climate change projections.

5. Summary and conclusions

Observations of daily maximum temperature and monthly precipitation and their counterpart fields from three coupled models from the CMIP3 archive have been used to examine the behavior of drought, heat waves, and their joint occurrence across the southern Africa subcontinent. Heat waves were defined when daily Tx values exceeded the 90th percentile for at least 3 consecutive days while drought was identified via a standardized index of seasonal precipitation. Using the observational data the occurrence of heat waves was evaluated first in isolation (unconditional probability of occurrence) and then conditioned on the concomitant occurrence of drought or El Niño conditions. These results were compared with similar behavior in three coupled models based on 20C3M runs for a common analysis period of 1961–2000.

When evaluated across the study domain the coupled models were able to generate heat wave and drought relationships that were generally similar to those found in observations. This included an ability to generate similar unconditional heat wave probabilities and conditional probabilities based on the existence of drought conditions. The conditional probabilities for heat waves were found to be greater than their unconditional values in both models and observations keeping with a priori expectations. The models displayed less fidelity in being able to generate heat waves as frequently as in observations during El Niño events. This is hypothesized

to be related to a weaker El Niño–drought teleconnection in the models vis-à-vis observations, as supported by an EOF analysis of the drought index and its relationship to tropical Pacific SSTs.

In climate projections the joint heat wave–drought relationship was generally similar to that of the observational period. However, when using the 1981–2000 base period to identify daily temperature percentile thresholds the projections across all the models indicate the unconditional probability of a heat wave increases by almost a factor of 4 by the end of the current century. This result appears consistent with an upward trend in DJF seasonal temperatures in the models of between 3° and 4°C over the same period. For precipitation, the three models indicated an increase in the frequency of drier-than-average conditions for DJF. However, this particular result showed substantial model sensitivity with some models indicating an increase in wetter-than-average conditions for the same time periods evaluated.

Overall, when evaluated across the domain of southern Africa (i.e., not considering differences in local behavior) the models used in this study appear to generally be capable of simulating the observed statistics of heat waves and their relationship to seasonal drought. ENSO teleconnections were less faithfully produced. A substantial increase in the frequency of summer heat waves in the coming century is a consistent result across the models, while changes in summer precipitation are less clear although the models evaluated here suggest an increase in drier-than-average conditions. Decreasing trends in EF in the models is consistent with other studies examining drought based on soil moisture rather than precipitation alone. While not considered in detail, important local variations in heat wave behavior were also identified. For example, in coastal locations (where large human populations are often located) it was found that local wind trajectories appear to play an important role in either inhibiting or contributing to heat waves in South Africa. In these locations the heat wave–drought relationship was comparatively weak. Generally speaking, onshore flow is associated with fewer heat waves along coasts while a land trajectory with attendant downslope flow (implied adiabatic warming) was identified for several heat wave events at coastal locations near strong topographic relief. These processes are not well represented in coarse-resolution climate models.

Acknowledgments. The modeling groups and the Program for Climate Model Diagnosis and Intercomparison (PCMDI) and the WCRP's Working Group on Coupled Modeling (WGCM) are acknowledged for their roles in making available the WCRP CMIP3 multimodel dataset. Support of this dataset is provided by the Office of Science, U.S. Department of Energy. Dr. Benno Blumenthal was instrumental in making the PCDMI data accessible via the IRI Data Library. The South African Weather Service kindly provided the daily maximum temperature data and the help of John del Corral and Simon Mason is gratefully acknowledged for making them accessible. Comments on the original version of this manuscript by Tony Barnston and three anonymous reviewers are also very much appreciated. This work was funded by a Small Grant for Exploratory Research from the National Science Foundation (NSF), Grant NSF-ATM 07-39256, and from the National Oceanic and Atmospheric Administration (NOAA) through Grant NA05OAR4311004. Any opinions, findings, and conclusions or recommendations expressed in this paper are those of the author and do not necessarily reflect the views of the NSF or NOAA.

REFERENCES

AchutaRao, K., and K. R. Sperber, 2006: ENSO simulation in coupled ocean-atmosphere models: Are the current models better? *Climate Dyn.,* **27,** 1–15.

Alexander, L. V., and Coauthors, 2006: Global observed changes in daily climate extremes of temperature and precipitation. *J. Geophys. Res.,* **111,** D05109, doi:10.1029/2005JD006290.

Argaud, L., and Coauthors, 2007: Short- and long-term outcomes of heatstroke following the 2003 heat wave in Lyon, France. *Arch. Intern. Med.,* **167,** 2177–2183.

Basu, R., and J. M. Samet, 2002: Relationship between elevated ambient temperature and mortality: A review of the epidemiologic evidence. *Epidemiol. Rev.,* **24,** 190–202.

Changnon, S. A., K. E. Kunkel, and B. C. Reinke, 1996: Impacts and responses to the 1995 heat wave: A call to action. *Bull. Amer. Meteor. Soc.,* **77,** 1497–1506.

Déry, S. J., and E. F. Wood, 2005: Observed twentieth century land surface air temperature and precipitation covariability. *Geophys. Res. Lett.,* **32,** L21414, doi:10.1029/2005GL024234.

Dilley, M., and B. N. Heyman, 1995: ENSO and disaster: Droughts, floods and El Niño/Southern Oscillation warm events. *Disasters,* **19,** 181–193.

Halpert, M. S., and C. F. Ropelewski, 1992: Surface temperature patterns associated with the Southern Oscillation. *J. Climate,* **5,** 577–593.

Held, I. M., and B. J. Soden, 2006: Robust response of the hydrological cycle to global warming. *J. Climate,* **19,** 5686–5699.

Huang, J., and H. M. van den Dool, 1993: Monthly precipitation—Temperature relations and temperature prediction over the United States. *J. Climate,* **6,** 1111–1132.

Hughes, W. S., and R. C. Balling Jr., 1996: Urban influences on South African temperature trends. *Int. J. Climatol.,* **16,** 935–940.

Jones, P. D., and A. Moberg, 2003: Hemispheric and large-scale surface air temperature variations: An extensive revision and an update to 2001. *J. Climate,* **16,** 206–223.

Kalkstein, L. S., and R. E. Davis, 1989: Weather and human mortality: An evaluation of demographic and interregional

responses in the United States. *Ann. Assoc. Amer. Geogr.,* **79,** 44–64.

Kay, R. N. B., 1997: Responses of African livestock and wild herbivores to drought. *J. Arid Environ.,* **37,** 683–694.

Kenyon, J., and G. C. Hegerl, 2008: Influence of climate variability on global temperature extremes. *J. Climate,* **21,** 3872–3889.

Kistler, R., and Coauthors, 2001: The NCEP–NCAR 50-Year Reanalysis: Monthly means CD-ROM and documentation. *Bull. Amer. Meteor. Soc.,* **82,** 247–267.

Koster, R., S. Schubert, and M. Suarez, 2009: Analyzing the concurrence of meteorological droughts and warm periods, with implications for the determination of evaporative regime. *J. Climate,* **22,** 3331–3341.

Kruger, A. C., and S. Shongwe, 2004: Temperature trends in South Africa: 1960–2003. *Int. J. Climatol.,* **24,** 1929–1945.

Lyon, B., 2004: The strength of El Niño and the spatial extent of tropical drought. *Geophys. Res. Lett.,* **31,** L21204, doi:10.1029/2004GL020901.

——, and A. G. Barnston, 2005: ENSO and the spatial extent of interannual precipitation extremes in tropical land areas. *J. Climate,* **18,** 5095–5109.

——, and S. J. Mason, 2007: The 1997–98 summer rainfall season in southern Africa. Part I: Observations. *J. Climate,* **20,** 5134–5148.

Madden, R. A., and J. Williams, 1978: The correlation between temperature and precipitation in the United States and Europe. *Mon. Wea. Rev.,* **106,** 142–147.

Mason, S. J., and P. D. Tyson, 2000: The occurrence and predictability of droughts over Southern Africa. *Drought: A Global Assessment,* D. A. Wilhite, Ed., Vol. 1, Routledge, 113–134.

McKee, T. B., N. J. Doesken, and J. Kleist, 1993: The relationship of drought frequency and duration to time scales. Preprints, *Eigth Conf. on Applied Climatology,* Anaheim, CA, Amer. Meteor. Soc., 179–184.

Meehl, G. A., and C. Tebaldi, 2004: More intense, more frequent, and longer-lasting heat waves in the 21st century. *Science,* **305,** 994–997.

Parmesan, C., T. L. Root, and M. R. Willig, 2000: Impacts of extreme weather and climate on terrestrial biota. *Bull. Amer. Meteor. Soc.,* **81,** 443–450.

Ropelewski, C. F., and M. S. Halpert, 1987: Global and regional scale precipitation patterns associated with the El Niño/Southern Oscillation. *Mon. Wea. Rev.,* **115,** 1606–1626.

Rudolf, B., and F. Rubel, 2005: Global precipitation. *Observed Global Climate: New Series on Landolt–Bornstein, Numerical Data and Functional Relationships,* M. Hantel, Ed., Springer, 11.1–11.53.

Shefield, J., and E. F. Wood, 2008: Projected changes in drought occurrence under future global warming from multi-model, multi-scenario, IPCC AR4 simulations. *Climate Dyn.,* **31,** 79–105.

Sivakumar, M. V. K., 2006: Climate prediction and agriculture: Current status and future challenges. *Climate Res.,* **33,** 3–17.

Smith, T. M., and R. W. Reynolds, 2004: Improved extended reconstruction of SST. *J. Climate,* **17,** 2466–2477.

Solomon, S., D. Qin, M. Manning, M. Marquis, K. Averyt, M. M. B. Tignor, H. L. Miller Jr., and Z. Chen, Eds., 2007: *Climate Change 2007: The Physical Sciences Basis*. Cambridge University Press, 996 pp.

Tadross, M., C. Jack, and B. Hewitson, 2005: On RCM-based projections of change in southern Africa summer. *Geophys. Res. Lett.,* **32,** L23713, doi:10.1029/2005GL024460.

Trenberth, K. E., and D. J. Shea, 2005: Relationships between precipitation and surface temperature. *Geophys. Res. Lett.,* **32,** L14703, doi:10.1029/2005GL022760.

Wang, G., 2005: Agricultural drought in a future climate: Results from 15 global climate models participating in the IPCC 4th assessment. *Climate Dyn.,* **25,** 739–753.

Wilhite, D. A., 2000: *Drought: A Global Assessment*. Vol. 1. Routledge, 396 pp.

Wilks, D. S., 1995: *Statistical Methods in the Atmospheric Sciences*. Academic Press, 467 pp.